PHYSICAL REVIEW B **108**, 014304 (2023)

First-principles prediction of phase transition of YCo$_5$ from self-consistent phonon calculations

Guangzong Xing,* Yoshio Miura, and Terumasa Tadano†
Research Center for Magnetic and Spintronic Materials, National Institute for Materials Science, Tsukuba, Ibaraki 305-0047, Japan

(Received 6 January 2023; accepted 10 July 2023; published 20 July 2023)

A recent theoretical study has shown that hexagonal YCo$_5$ is dynamically unstable and distorts into a stable orthorhombic structure. In this paper, we show theoretically that the orthorhombic phase is energetically more stable than the hexagonal phase in the low-temperature region, while the phonon entropy stabilizes the hexagonal phase thermodynamically in the high-temperature region. The orthorhombic-to-hexagonal phase transition temperature is ∼165 K, which is determined using self-consistent phonon calculations. We investigate the magnetocrystalline anisotropy energy (MAE) using self-consistent and non-self-consistent (force theorem) calculations with spin-orbit interaction (SOI) along with the Hubbard U correction. Then, we find that the orthorhombic phase has MAE, orbital moment, and orbital moment anisotropy values that are similar to those of the hexagonal phase when the self-consistent calculation with SOI is performed. Since the orthorhombic phase still gives magnetic properties comparable to those found in experiments, the orthorhombic distortion is potentially realized in the low-temperature region, which awaits experimental exploration.

DOI: 10.1103/PhysRevB.108.014304

I. INTRODUCTION

CaCu$_5$-type RCo$_5$ (R = rare earth) intermetallic compounds have emerged as promising permanent magnets owing to their high Curie temperature, high saturation magnetization, and strong coercivity [1–5]. The coercivity is related to the intrinsic properties of a material, namely, the magnetocrystalline anisotropy energy (MAE), which can be obtained by measuring the energy difference along different directions of magnetization with respect to the crystal axes [6–9]. Among the members of the RCo$_5$ family, the magnetic properties of YCo$_5$ have been extensively studied both from experiments and using first-principles methods based on density functional theory (DFT) [4,10]. A saturated magnetization of ∼910 emu/cm^3, a magnetocrystalline anisotropy constant of 7.38×10^7 erg/cm^3 at 4.2 K, and a Curie temperature of 977 K were obtained in Ref. [8]. Previous studies indicate that DFT calculations at the level of the local density approximation (LDA) or the generalized gradient approximation (GGA) significantly underestimate the orbital magnetic moments of Co atoms and the MAE in comparison with experimental values. These underestimation problems have been tackled by including the orbital polarization scheme [11,12] or by using DFT+U [13,14] or LDA + dynamical mean-field theory (LDA+DMFT) [15] approaches.

All of the previous theoretical calculations have been performed using the CaCu$_5$-type structure [Fig. 1(a)], which displays a layered hexagonal lattice (space group $P6/mmm$) with two different kinds of Co atoms labeled as Co$_{2c}$ and Co$_{3g}$ [16]. However, a recent first-principles study has shown that a phonon at the L point of the first Brillouin zone is dynamically unstable at 0 K [17], indicating that the hexagonal phase distorts into a lower-energy phase, as schematically illustrated in Fig. 1(d). Indeed, Ref. [17] has reported that the distorted orthorhombic phase (space group $Imma$) is energetically more stable than the hexagonal phase. Given the presence of the double-well potential energy surface of the unstable phonon mode [Fig. 1(d)], there should be a structural phase transition induced by the soft phonon excited at finite temperatures. Since the magnetic properties, such as the MAE, are sensitive to the crystal structure, understanding the temperature evolution of the crystal structure is crucial for reliably comparing the magnetic properties of YCo$_5$ obtained from theory and experiments.

Here, by using the state-of-the-art anharmonic phonon calculation method, we demonstrate that the orthorhombic-to-hexagonal phase transition of YCo$_5$ can take place with heating. We first show that the orthorhombic phase is predicted to be *energetically* more stable than the hexagonal phase at 0 K with various exchange-correlation (XC) functionals, including GGA, GGA+U, the strongly constrained and appropriately normed meta-GGA (SCAN), and the Heyd-Scuseria-Ernzerhof hybrid functional (HSE06). As the temperature rises, the hexagonal phase becomes *thermodynamically* more stable than the orthorhombic phase at ∼165 K, which is estimated from the Helmholtz free energies computed using the self-consistent phonon method [18,19]. The MAE values of both phases computed using the force theorem, which is a non-self-consistent calculation with the spin-orbit interaction (SOI), within GGA underestimate the experimental values, whereas a self-consistent calculation with the SOI under the GGA+U scheme yields larger MAE values comparable to experiments. By contrast, the MAE values in the orthorhombic phase obtained by the force theorem within GGA+U still fall short of experimental values for all the applied U values. We attribute this to the fact that both the

---

*XING.Guangzong@nims.go.jp
†TADANO.Terumasa@nims.go.jp

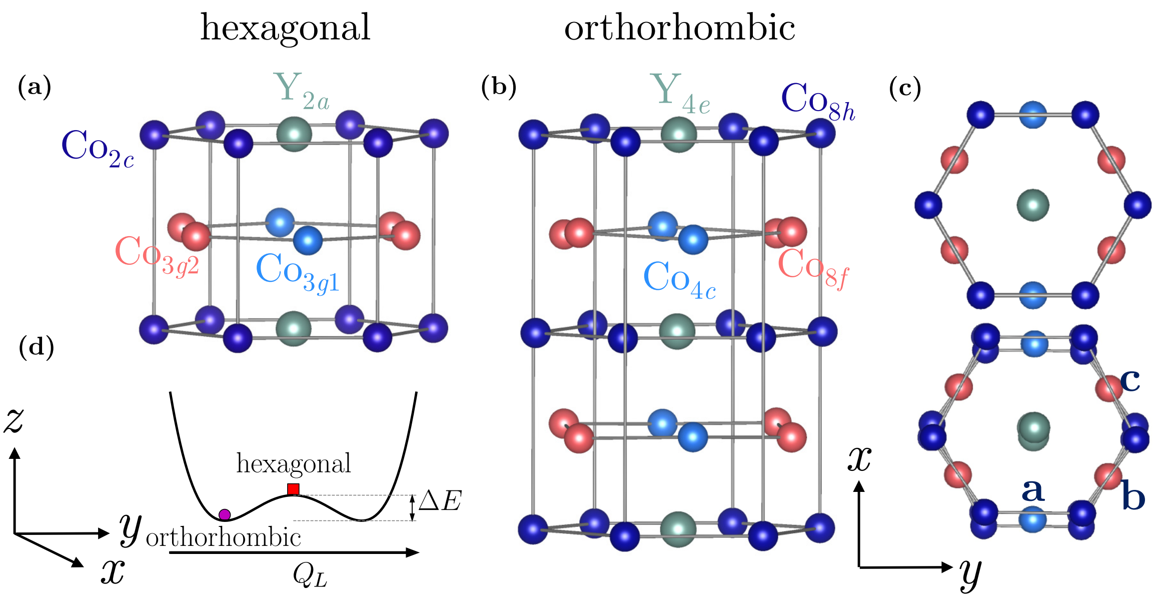

FIG. 1. Crystal structure of the hexagonal (a) and orthorhombic (b) phases of $\mathrm{YCo_5}$. The Y and Co atoms are represented by the large and small spheres, respectively. The atomic Wyckoff position for different atoms is marked with the corresponding colors. (c) Top view of the crystal structures of hexagonal (top panel) and orthorhombic (lower panel) $\mathrm{YCo_5}$. (d) Schematic diagram of the double-well potential obtained by displacing atoms along the direction of the L-point soft phonon mode of the hexagonal phase. Q_L is the normal coordinate amplitude, and ΔE represents the static energy difference between the two phases.

orbital moment of $\sim 0.1\ \mu_\mathrm{B}$ and the orbital moment anisotropy (OMA) with a value of $\sim 0.03\ \mu_\mathrm{B}$, which is proportional to the MAE, at the Co site were significantly underestimated by the force theorem compared with the corresponding experimentally measured values of $\sim 0.2\ \mu_\mathrm{B}$ [15] and $\sim 0.06\ \mu_\mathrm{B}$ [8], respectively.

The structure of this paper is as follows. The theoretical approach to calculate the MAE and the computational details are described in Secs. II A and II B, respectively. The main results are shown in Sec. III. The orthorhombic-to-hexagonal phase transition induced by lattice anharmonicity is discussed in Sec. III A. In Sec. III B, we evaluate the MAE for both phases using both the force theorem and self-consistent methods within the GGA+U. Finally, we summarize the study in Sec. IV.

II. METHODS

A. MAE from DFT calculation

The MAE at 0 K was evaluated based on DFT as

$$K_\mathrm{u}^\mathrm{DFT} = E_{0,\perp} - E_{0,\parallel}, \tag{1}$$

where $E_{0,\perp}$ and $E_{0,\parallel}$ are the ground state total energies with the magnetic moment $\boldsymbol{m}$ being aligned along the hard and easy axes, respectively. These energies were computed by performing DFT calculations with the SOI using the force theorem [20] (a non-self-consistent approach) and self-consistent approaches. The easy axis for both phases was found along the [001] direction ($\boldsymbol{m} \parallel \boldsymbol{c}$). To determine the hard axis, we calculated the total energy by varying the azimuthal angle ϕ in the basal plane ($\boldsymbol{m} \perp \boldsymbol{c}$) from 0 to 2π with a step of $\frac{\pi}{6}$. The energy difference between different ϕ in the hexagonal phase was negligible. In the orthorhombic phase, the maximum energy difference was $\sim 0.4\ \mathrm{MJ/m^3}$ with the lowest energy at $\phi = \frac{\pi}{2}$ ([010] direction). Therefore we employed the hard axis along the [100] direction for the hexagonal phase and along the [010] direction for the orthorhombic phase to obtain $K_\mathrm{u}^\mathrm{DFT}$. Although the choice of the hard axis may slightly affect the MAE, the small energy difference does not affect the overall conclusion.

According to the Bruno relation [21], MAE is proportional to the OMA defined as

$$\Delta m_\mathrm{o} = m_{\mathrm{o},\parallel}^\mathrm{Co} - m_{\mathrm{o},\perp}^\mathrm{Co}, \tag{2}$$

where $m_{\mathrm{o},\parallel}^\mathrm{Co}$ and $m_{\mathrm{o},\perp}^\mathrm{Co}$ are the orbital magnetic moment at the Co site along the easy and hard axes, respectively.

B. Computational details

The DFT calculations in this paper were performed mainly by using the projector augmented wave (PAW) method [22], as implemented in the Vienna *ab initio* simulation package (VASP) code (version 6.2.1) [23]. The recommended set of PAW potentials, which accounts for the scalar relativistic effect, was used. A kinetic-energy cutoff of 400 eV and a k-point mesh density of $\sim 450\ \text{Å}^3$ were employed. We adopted the second-order Methfessel-Paxton [24] (MP) smearing method with a width of 0.2 eV for structural optimization. A much denser k-mesh density of $\sim 6000\ \text{Å}^3$ and the tetrahedron method with the Blöchl correction [25] were employed to calculate the static energy difference $\Delta E = E_0^\mathrm{orth} - E_0^\mathrm{hex}$ between the orthorhombic and hexagonal phases, the MAE, the density of states (DOS), and the crystal orbital Hamilton populations (COHPs). For these calculations, the initial local moments of $3\ \mu_\mathrm{B}$ and $-0.3\ \mu_\mathrm{B}$ were used for the Co and Y atoms, respectively. The SOI was also included in the MAE calculation. The subsequent phonon calculations were performed within the GGA by Perdew, Burke, and Ernzerhof

(GGA-PBE) [26] without the Hubbard U correction for the following reasons. First, as we elaborate below, we confirmed that the orthorhombic phase is energetically more stable at 0 K, irrespective of the XC functionals. Second, phonon frequencies are sensitive to the employed lattice parameters, and GGA-PBE yields lattice parameters of the hexagonal phase that are in accord with experimental values [27] within an error of ~1%. Lastly, we encountered technical challenges in achieving convergences when applying GGA+U functionals for displaced supercells. Although repeated adjustments to the mixing parameters could achieve convergence, the calculated potential energy surface was not smooth enough to obtain reliable harmonic force constants.

It has been reported that MAE obtained using GGA-PBE significantly underestimated the experimental values. To address the underestimation problem, we employ the GGA+U scheme [28] to account for the correlation effect of the Co-3d electrons. To compute the total energies under the GGA+U scheme with the SOI, we employed two different approaches: self-consistent (SC) and force theorem (FT) calculations. The main difference is whether the charge density from the self-consistent spin-polarized calculation is updated self-consistently or not; in the SC method, the charge density is optimized again, whereas it is not so in the FT. Additionally, we employed the full-potential linearized augmented plane-wave (FLAPW) method [29], as implemented in the WIEN2k code [30], to investigate the effect of the core electrons on the MAE and orbital moment of $\mathrm{YCo_5}$. The crystal structure optimized using VASP within GGA-PBE was adopted to calculate the MAE, the OMA, and the orbital moment. We used atomic sphere radii of 2.015 and 2.115 bohr for Co and Y, respectively, and a basis set cutoff parameter of $R_{\mathrm{min}}K_{\mathrm{max}} = 9$.

To compute the vibrational Helmholtz free energy F_{vib} within the first-order self-consistent phonon (SCP) theory, second-order and fourth-order interatomic force constants (IFCs) are required. A $2 \times 2 \times 2$ supercell containing 48 (96) atoms was used for calculating the second-order IFCs of the hexagonal (orthorhombic) phase. Here, each atom in the supercell was displaced from its equilibrium position by 0.03 Å, and the atomic forces were calculated using VASP. From the generated displacement-force data set, we estimated the second-order IFCs by ordinary least squares. For anharmonic IFCs, a supercell containing 48 atoms was adopted for both phases. We employed the compressive sensing lattice dynamics to extract the anharmonic IFCs [31] from the displacement-force training data sets. Here, we uniformly sampled 200 training structures from the last 2500 steps of an *ab initio* molecular dynamics calculation (5000 steps in total) at 10 K for both phases. For each sampled structure, we further displaced all atoms by 0.1 Å in random directions. We have confirmed that 200 sample structures were sufficient and the change in $\Delta F_{\mathrm{vib}} = F_{\mathrm{vib}}^{\mathrm{orth}} - F_{\mathrm{vib}}^{\mathrm{hex}}$ between the orthorhombic and hexagonal phases after adding 50 more structures (250 structures in total) was smaller than ~0.5 meV/f.u. at 500 K. In our phonon calculations based on GGA-PBE, we found that the harmonic phonon dispersion of the hexagonal phase is sensitive to the broadening parameter σ of the MP method used for the IFC calculations, which is particularly noticeable when $\sigma \gtrsim 0.1$ eV. Thus we carefully investigated the σ dependence of the predicted structural transition temperature T_{c} and found that σ as small as 0.085 eV was desirable for obtaining a converged T_c value. We discuss this point in Sec. III A. All the phonon calculations in this paper were performed using the ALAMODE code [19,32].

TABLE I. Calculated static electronic energy difference (ΔE; see text) between the hexagonal and orthorhombic phases and the squared frequency of the soft mode at the L point (ω_L^2) for hexagonal $\mathrm{YCo_5}$ using different XC functionals.

XC functional	ΔE (meV/f.u.)	ω_L^2 (cm^{-2})
LDA	−44.08	−7826.4
PBE	−23.24	−4301.2
PBEsol	−23.78	−4425.9
GGA+U ($U = 1$ eV)	−52.39	
SCAN	−97.31	
HSE06	−134.48	

III. RESULTS AND DISCUSSION

A. Phase transition induced by lattice anharmonicity

First, to assess the stability of the hexagonal and orthorhombic phases at 0 K, we calculated the ground state energies using various XC functionals: LDA [33], PBE, its variant for solids (PBEsol) [34], GGA+U [28] with $U = 1$ eV, the strongly constrained and appropriately normed meta-GGA (SCAN) [35], and the Heyd-Scuseria-Ernzerhof hybrid functional (HSE06) [36]. For each XC functional other than HSE06, the crystal structures of the two phases were fully relaxed with the collinear ferromagnetic spin configuration. The detailed structural parameters are listed in Tables S1 and S2 of the Supplemental Material (SM) [37]. For HSE06, the crystal structures from the PBE calculation were used. The difference of the ground state energies $\Delta E = E_0^{\mathrm{orth}} - E_0^{\mathrm{hex}}$, with E_0^X being the energy of phase X per formula unit (f.u.), is summarized in Table I. It is clear that the orthorhombic phase is predicted to be energetically more stable at 0 K irrespective of the employed XC functionals. In the following, the crystal structures for both phases optimized by GGA-PBE are used to perform further phonon and magnetic property calculations except for the squared frequency ω_L^2 of the soft mode tabulated in Table I, for which the crystal structures optimized by each XC functional are used.

Next, we discuss the thermodynamic stability of the two phases at finite temperatures by comparing the Helmholtz free energies defined as

$$F(V, T) = E_0(V_0) + F_{\mathrm{vib}}(V, T) + F_{\mathrm{el}}(V, T), \tag{3}$$

where $E_0(V)$ is the static electronic energy obtained from a conventional DFT calculation and $F_{\mathrm{el}}(V, T)$ and $F_{\mathrm{vib}}(V, T)$ are the electronic and vibrational free energies at temperature T and cell volume V. Since the lattice constants reportedly increase only by ~0.04 Å at 600 K [27], we neglect the thermal expansion effect and use the optimized cell volume V_0 at 0 K for computing the Helmholtz free energy. Also, since a magnetic phase transition, e.g., an anomaly in the heat capacity, has never been observed in the low-temperature region, the magnetic entropy is also omitted in this paper assuming that the difference in magnetic entropy between the two phases is negligible. Then, the electronic free energy $F_{\mathrm{el}}(V_0, T)$ and vibrational free energy $F_{\mathrm{vib}}(V_0, T)$ play a central role in determining the thermodynamic stability. F_{el} is obtained based on the fixed density-of-states approximation [38,39]. When all phonon modes are dynamically stable within the harmonic approximation (HA), it is straightforward to estimate $F_{\mathrm{vib}}(V_0, T)$. However, for the hexagonal YCo$_5$, the method based on the HA breaks down due to the presence of the soft mode at the L point. Hence, in this paper, we employ the SCP scheme. In this approach, we first compute finite-temperature phonon frequencies by solving the following SCP equation [40,41]:

$$\Omega_q^2 = \omega_q^2 + \frac{1}{2}\sum_{q_1}\Phi(q;-q;q_1;-q_1)\alpha_{q_1}. \tag{4}$$

Here, ω_q is the angular frequency of the phonon mode q obtained within the HA, Ω_q is the frequency at finite temperature renormalized by the anharmonic interaction $\Phi(q;-q;q_1;-q_1)$ associated with the fourth-order anharmonicity of the potential energy surface, and $\alpha_q = \frac{\hbar}{2\Omega_q}[1 + 2n(\Omega_q)]$ with $n(\omega)$ being the Bose-Einstein distribution function. Once the above equation is solved for Ω_q, the vibrational free energy can be evaluated as $F_{\mathrm{vib}}^{(\mathrm{SCP})}(V_0, T) = \tilde{F}_{\mathrm{vib}}^{(\mathrm{QHA})}(V_0, T) + \Delta F_{\mathrm{vib}}^{\mathrm{corr}}(V_0, T)$, which is the sum of the quasiharmonic (QH) term computed using Ω_q and the correction term necessary to satisfy the correct thermodynamic relationship of $-dF_{\mathrm{vib}}/dT = S_{\mathrm{vib}}$ [42,43]. More details of the mathematical expressions for $F_{\mathrm{vib}}^{(\mathrm{SCP})}$ can be found in the SM [37].

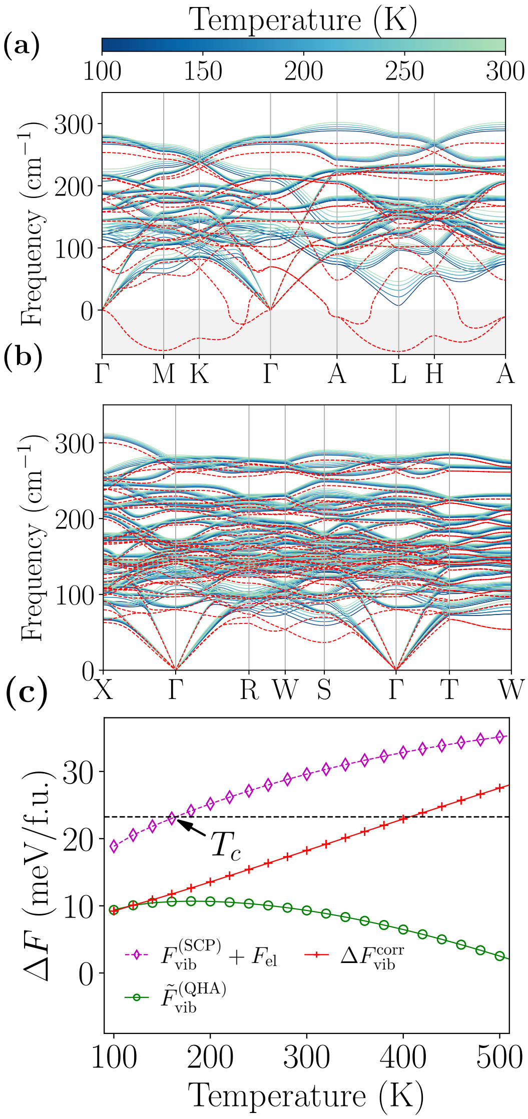

FIG. 2. Temperature-dependent anharmonic phonon dispersion of hexagonal (a) and orthorhombic (b) phases of YCo$_5$. The color map shows the self-consistent phonon solutions in the temperature range 100–300 K, and the dashed curves are harmonic lattice dynamics results. Imaginary frequency is shown as negative. (c) Calculated difference of the free energies, $\Delta F(T)$ (see text). The horizontal dashed line is the difference of the static energies $-\Delta E = 23.24$ meV/f.u. Here, the phonon calculations are performed with $\sigma = 0.075$ eV.

Figures 2(a) and 2(b) show the phonon dispersion curves of hexagonal and orthorhombic YCo$_5$ within the HA (dashed curves) and SCP theory (solid curves). The SCP frequencies from 100 to 300 K in steps of 50 K are shown with different colors. It is clear that the harmonic phonon of the hexagonal YCo$_5$ is dynamically unstable with the most unstable mode occurring at the L points. This instability was also observed with other XC functionals, as indicated by the negative ω_L^2 values in Table I. By contrast, the harmonic phonon is dynamically stable for the distorted orthorhombic phase [see Fig. 2(b)]. The soft modes of the hexagonal phase at the L and M points mainly involve the in-plane [xy plane in Fig. 1(c)] displacements of the Co$_{2c}$ atoms together with relatively small displacements of the other atoms. Recently, it has been shown that the phonon instability at the L point originates from the strong antibonding nature of the Co$_{2c}$-Co$_{2c}$ bond [17], as evidenced by a sharp peak in the crystal orbital Hamilton populations (COHPs) [44] near the Fermi level. To see how the antibonding nature changes with the structural distortion, we compare the calculated −COHP values in Fig. 3(a). The originally equidistant Co$_{2c}$-Co$_{2c}$ bonds split into three different Co$_{8h}$-Co$_{8h}$ bonds labeled as a, b, and c [see bottom panel of Fig. 1(c)], with the corresponding bond lengths of 2.75, 2.57, and 3.21 Å, respectively. Hence the −COHP values for the three inequivalent Co$_{8h}$-Co$_{8h}$ bonds are averaged here. Compared with the large population of antibonding states [red curve in Fig. 3(a)] at the Fermi energy in hexagonal YCo$_5$, the magnitude of −COHP in the orthorhombic phase is reduced significantly, which can be explained by the smaller projected DOS [Fig. 3(b)] of the $d_{x^2-y^2}$ orbital at the Co$_{8h}$ sites. Such a large reduction in the −COHP value by structural distortion is consistent with the trend of phonon stability we observed. Interestingly, the projected DOS in Fig. S1 of the SM [37] shows that the peak of the Co$_{2c}$ $d_{x^2-y^2}$ orbital at the Fermi energy does not change appreciably even when we used the SCAN functional and GGA+U with various U parameters. This suggests the presence of phonon instability in the hexagonal YCo$_5$ even with XC functionals other than GGA-PBE, in accord with the trend of ΔE shown in Table I.

As can be seen in Figs. 2(a) and 2(b), the phonon frequencies significantly increase by the quartic anharmonicity

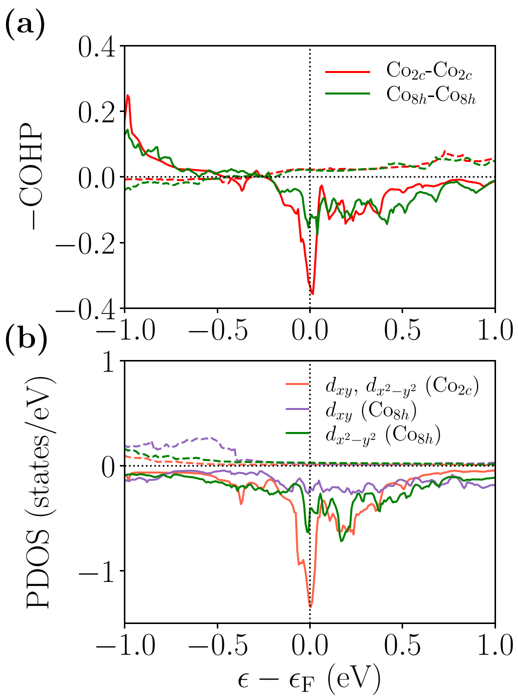

FIG. 3. (a) Crystal orbital Hamilton population (COHP) calculation of the Co$_{2c}$-Co$_{2c}$ bond in the hexagonal phase and Co$_{8h}$-Co$_{8h}$ bond in the orthorhombic phase. (b) Projected density of states (PDOS) for 3d states at the Co$_{2c}$ and Co$_{8h}$ sites. The solid and dashed curves represent the minority and majority spin states, respectively. The data for hexagonal YCo$_5$ are adapted from Ref. [17].

at finite temperatures, which is particularly notable in the low-energy optical modes. Since SCP theory postulates the renormalized phonons to be stable in Eq. (4), we observe that the finite-temperature phonons are stable irrespective of the temperature for both phases. Hence the information of the self-consistent phonon dispersion alone cannot determine the structural phase transition temperature T_c reliably [45,46]. In this paper, we employ another approach based on Eq. (3), where T_c is estimated from the difference in the electronic and vibrational free energies defined as $\Delta F(T) = F_{\rm vib}^{\rm orth}(T) + F_{\rm el}^{\rm orth}(T) - [F_{\rm vib}^{\rm hex}(T) + F_{\rm el}^{\rm hex}(T)]$. The calculated $\Delta F(T)$ is shown in Fig. 2(c). The increase in ΔF with heating occurs because the electronic and vibrational entropy gradually enhances the stability of the hexagonal phase. Eventually, the hexagonal phase becomes more stable when $F^{\rm hex}(T) \leqslant F^{\rm orth}(T)$, or equivalently $-\Delta E \leqslant \Delta F(T)$, is satisfied. From this condition, a T_c value of ∼165 K was obtained when evaluating $\Delta F(T)$ using the MP method with the broadening parameter σ of 0.075 eV, as shown in Fig. 2(c). While a magnetoelastic study showed the hexagonal phase to be stable down to ∼100 K under hydrostatic pressure [47,48], a detailed structure analysis at ambient pressure below ∼165 K is necessary to test the present prediction.

Here, we discuss the dependency of $T_{\rm c}$ on the employed σ value. As shown in Fig. S2 of the SM [37], the harmonic phonon dispersion of the hexagonal phase was sensitive to the σ value, particularly noticeable near the A $(0, 0, \frac{1}{2})$ point of the Brillouin zone. By contrast, we did not observe such a significant σ dependence for the phonon dispersion of the orthorhombic phase. These different behaviors are consistent with the large difference in the projected DOS at the Fermi level, shown in Fig. 3(b). Interestingly, in the case of anharmonic phonon calculations, the phonon frequencies were not so sensitive to σ even for the hexagonal phase. This occurred presumably because the relatively large and random displacements we used for computing anharmonic IFCs lifted the degeneracy and thereby reduced the DOS at the Fermi level, making the anharmonic IFCs less sensitive to σ. Because of the observed σ dependency of the phonon frequencies, the $\Delta F(T)$ value also changed slightly with σ, leading to a sizable shift in $T_{\rm c}$, as shown in Fig. S3(b) of the SM [37]. With decreasing σ from 0.2 to 0.085 eV, $T_{\rm c}$ gradually decreased from ∼240 to ∼165 K. In the smaller-σ region of 0.060–0.085 eV, the calculated $T_{\rm c}$ value remained nearly constant at ∼165 K, indicating convergence of the calculation with respect to σ. We also confirmed that a σ value as small as 0.085 eV can give a potential energy surface of the third mode at the A point which agrees almost perfectly with that computed using the tetrahedron method with the Blöchl correction, whereas a larger σ overestimated the Hessian, as shown in Fig. S2(b) of the SM [37].

B. MAE for two phases

In the following, we compare the MAE values of the two phases obtained from two different approaches: FT [20], i.e., a non-self-consistent calculation with the SOI, and SC calculations with the SOI. For the hexagonal phase, the MAE value, defined as $K_{\rm u}^{\rm DFT} = E_{0,\perp} - E_{0,\parallel}$, was 0.75 MJ/m^3 within GGA-PBE, which significantly underestimates the experimental values of ∼7.4 MJ/m^3 [8] and ∼6.0 MJ/m^3 [9]. This underestimation problem could be resolved by adding the Hubbard U correction. Zhou and Ozoliņš [49] reported that the GGA+U method does not adequately describe the orbital ground state for strongly correlated f-electron systems due to the significant anisotropy in the self-interaction error (SIE) of the f orbitals. However, in YCo$_5$ without f electrons, the 3d electrons of Co are more itinerant and less correlated, and the SIE anisotropy should be less significant in comparison with the typical energy scale of the crystal field and bandwidth [11,50]. Therefore the GGA+U method is still valid for calculating the MAE and orbital moment, which has been demonstrated in previous GGA+U studies on some Co compounds [51,52].

For hexagonal YCo$_5$, our FT calculation in Fig. 4(a) nicely reproduced the U dependence of the MAE from a previous FT result based on GGA+U [13], and the $K_{\rm u}^{\rm DFT}$ value became comparable with the experimental values when $U \sim 1.75$ eV. However, at this U value, the FT still underestimated the total orbital moments and their anisotropy (OMA), $\Delta m_{\rm o} = m_{{\rm o},\parallel}^{\rm Co} - m_{{\rm o},\perp}^{\rm Co}$, for all Co sites, as shown in Figs. 4(c) and 4(b), respectively. We observed that the SC approach can yield MAE and orbital moment results that are much more consistent with experimental values, as we elaborate below. The SC scheme enhanced the $K_{\rm u}^{\rm DFT}$ values at all the U values, as shown in Fig. 4(a). Consequently, an agreement with experimental values was obtained for the MAE at $U \sim 0.75$ eV, which is smaller than the U of ∼1.75 eV for the FT approach.

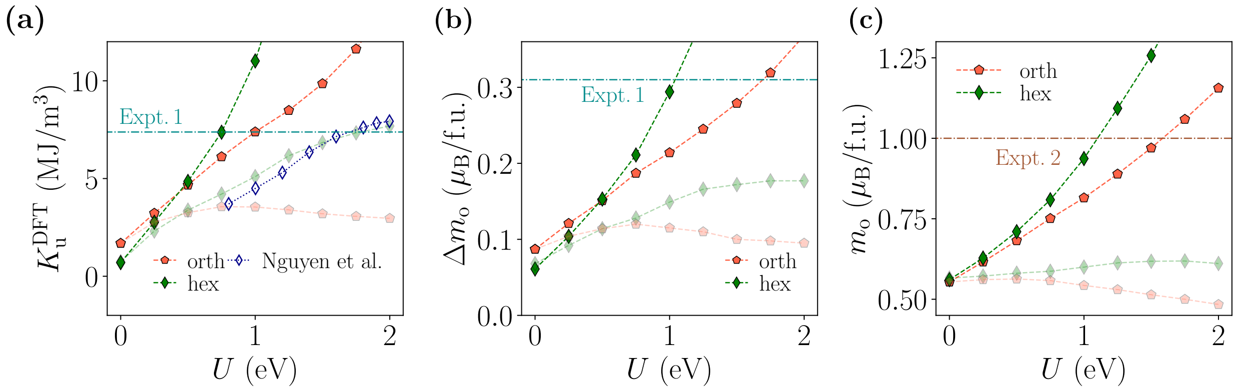

FIG. 4. Dependence of magnetocrystalline anisotropy energy K_u^{DFT} (a), orbital moment anisotropy Δm_o (b), and orbital moment m_o (c) for the hexagonal and orthorhombic phases of YCo$_5$ under the GGA+U scheme. The solid and translucent symbols represent the quantities mentioned above obtained using the self-consistent and force theorem approaches, respectively. The unfilled diamonds show the theoretical results from Nguyen *et al.* [13] based on the force theorem, and the horizontal dash-dotted lines, labeled as Expt. 1, and Expt. 2, show the experimental results from Ref. [8] and Ref. [15], respectively. Note that the Δm_o and m_o of the Y atom are not included in (b) and (c) for comparison with the experimental data.

At $U = 0.75$ eV, the SC approach gave an orbital moment of $\sim$0.8 μ_B/f.u., in better agreement with the experimental value of $\sim$1 μ_B/f.u. [15] [see Fig. 4(c)]. Although perfect agreements in the MAE, orbital moment, and OMA were not reached simultaneously with a single U value, it is clear that the SC scheme gives more reliable results than the FT approach.

For the orthorhombic phase, we obtained U-dependent MAE, OMA, and orbital moment values which were qualitatively similar to those of the hexagonal phase when the SC approach was used, as shown by the filled markers in Figs. 4(a), 4(b), and 4(c). One minor difference can be found in the U value to reproduce the experimental MAE; for the orthorhombic phase, a slightly larger U value of $\sim$1.0 eV appears to give essentially the same magnetic properties as the hexagonal phase. Even at $U = 0.75$ eV, which was applied to the hexagonal phase, the MAE of 6.12 MJ/m^3 still reaches the range of experimental observations (6.0–7.4 MJ/m^3). Interestingly, we found that the FT failed completely for the orthorhombic phase, as inferred from the consistently lower MAE values in Fig. 4(a), which can be attributed to the underestimation of the OMA [Fig. 4(b)]. In the context of the GGA+U scheme with the SOI, the FT approach only modifies the GGA energy due to the Coulomb interaction between the Co-3d electrons occupying the same ion. However, the change in occupancy due to the on-site electron-electron Coulomb interaction is neglected because the charge density is not self-consistently updated. Therefore it is reasonable that the FT calculations underestimate the orbital moment, the OMA, and, consequently, the MAE. We note that the SC approach could reproduce the experimentally observed larger orbital moments and OMA at the Co$_{2c}$ and Co$_{8h}$ sites than at the other Co sites for both of the two phases. The details of the site dependency are summarized in the SM [37]. In addition, the total spin and orbital magnetic moment obtained by the SC calculation with $U = 0.75$ eV ($U = 1.0$ eV) for the hexagonal (orthorhombic) phase is 8.44 μ_B/f.u. (8.52 μ_B/f.u.) and agrees well with the experimental values of $\sim$8.3 μ_B/f.u. [8] and $\sim$8.4 μ_B/f.u. [4], while the total moment of 7.80 μ_B/f.u. (7.73 μ_B/f.u.) determined without U underestimates the experimental results. We have confirmed that other GGA+U correction schemes [53–55] as well as a full-potential all-electron calculation [29,30] give quantitatively similar MAE values (please see details in the SM [37]).

IV. SUMMARY

To summarize, we have theoretically demonstrated a possible orthorhombic-to-hexagonal structural phase transition of YCo$_5$ induced by heating. We found that the orthorhombic phase is energetically more stable than the hexagonal phase at 0 K irrespective of the employed exchange-correlation functionals. The stable, temperature-dependent phonons of these phases were obtained by incorporating the anharmonic renormalization using the self-consistent phonon approach, and the theoretical phase transition temperature of $\sim$165 K was obtained by comparing the calculated Helmholtz free energies. We compared the MAE, the associated orbital moment anisotropy, and the orbital moments of the two phases computed using the force theorem and self-consistent calculations with the SOI based on the GGA+U scheme. We showed that the magnetic properties of the orthorhombic phase were similar to those of the hexagonal phase when the self-consistent approach was employed. Since the calculated magnetic properties also agreed well with the available experimental data, we expect the predicted orthorhombic phase to be existent in the low-temperature region, which awaits experimental verification.

ACKNOWLEDGMENTS

This work was partly supported by MEXT Program: Data Creation and Utilization-Type Material Research and Development Project (Digital Transformation Initiative Center for Magnetic Materials) Grant No. JPMXP1122715503. The figures showing crystal structures were created using VESTA software [56].

[1] C. E. Patrick and J. B. Staunton, Temperature-dependent magnetocrystalline anisotropy of rare earth/transition metal permanent magnets from first principles: The light $R\mathrm{Co}_5$ ($R =$ Y, La–Gd) intermetallics, Phys. Rev. Mater. **3**, 101401(R) (2019).

[2] S. Kumar, C. E. Patrick, R. S. Edwards, G. Balakrishnan, M. R. Lees, and J. B. Staunton, Torque magnetometry study of the spin reorientation transition and temperature-dependent magnetocrystalline anisotropy in NdCo_5, J. Phys.: Condens. Matter **32**, 255802 (2020).

[3] H. Ucar, R. Choudhary, and D. Paudyal, An overview of the first principles studies of doped RE-TM_5 systems for the development of hard magnetic properties, J. Magn. Magn. Mater. **496**, 165902 (2020).

[4] C. E. Patrick, S. Kumar, G. Balakrishnan, R. S. Edwards, M. R. Lees, E. Mendive-Tapia, L. Petit, and J. B. Staunton, Rare-earth/transition-metal magnetic interactions in pristine and (Ni,Fe)-doped YCo_5 and GdCo_5, Phys. Rev. Mater. **1**, 024411 (2017).

[5] O. Gutfleisch, M. A. Willard, E. Brück, C. H. Chen, S. G. Sankar, and J. P. Liu, Magnetic materials and devices for the 21st century: Stronger, lighter, and more energy efficient, Adv. Mater. **23**, 821 (2011).

[6] J. Trygg, B. Johansson, O. Eriksson, and J. M. Wills, Total Energy Calculation of the Magnetocrystalline Anisotropy Energy in the Ferromagnetic 3*d* Metals, Phys. Rev. Lett. **75**, 2871 (1995).

[7] P. Błoński, A. Lehnert, S. Dennler, S. Rusponi, M. Etzkorn, G. Moulas, P. Bencok, P. Gambardella, H. Brune, and J. Hafner, Magnetocrystalline anisotropy energy of Co and Fe adatoms on the (111) surfaces of Pd and Rh, Phys. Rev. B **81**, 104426 (2010).

[8] J. M. Alameda, D. Givord, R. Lemaire, and Q. Lu, Co energy and magnetization anisotropies in RCo_5 intermetallics between 4.2 K and 300 K, J. Appl. Phys. **52**, 2079 (1981).

[9] J. Franse, N. Thuy, and N. Hong, Individual site magnetic anisotropy of the iron and cobalt ions in rare earth-iron and rare earth-cobalt intermetallic compounds, J. Magn. Magn. Mater. **72**, 361 (1988).

[10] P. Larson and I. Mazin, Calculation of magnetic anisotropy energy in YCo_5, J. Magn. Magn. Mater. **264**, 7 (2003).

[11] L. Steinbeck, M. Richter, and H. Eschrig, Itinerant-electron magnetocrystalline anisotropy energy of YCo_5 and related compounds, Phys. Rev. B **63**, 184431 (2001).

[12] G. H. O. Daalderop, P. J. Kelly, and M. F. H. Schuurmans, Magnetocrystalline anisotropy of YCo_5 and related RECo_5 compounds, Phys. Rev. B **53**, 14415 (1996).

[13] M. C. Nguyen, Y. Yao, C.-Z. Wang, K.-M. Ho, and V. P. Antropov, Magnetocrystalline anisotropy in cobalt based magnets: A choice of correlation parameters and the relativistic effects, J. Phys.: Condens. Matter **30**, 195801 (2018).

[14] A. Asali, J. Fidler, and D. Suess, Influence of changes in electronic structure on magnetocrystalline anisotropy of YCo_5 and related compounds, J. Magn. Magn. Mater. **485**, 61 (2019).

[15] J.-X. Zhu, M. Janoschek, R. Rosenberg, F. Ronning, J. D. Thompson, M. A. Torrez, E. D. Bauer, and C. D. Batista, LDA+DMFT Approach to Magnetocrystalline Anisotropy of Strong Magnets, Phys. Rev. X **4**, 021027 (2014).

[16] The threefold degenerate Co_{3g} atoms will be separated into two inequivalent sites with multiplicity of 1 (denoted as Co_{3g1}) and 2 (denoted as Co_{3g2}) when the magnetization is along the hard axis (the [100] direction).

[17] G. Xing, Y. Miura, and T. Tadano, Lattice dynamics and its effects on magnetocrystalline anisotropy energy of pristine and hole-doped YCo_5 from first principles, Phys. Rev. B **105**, 104427 (2022).

[18] D. Hooton, The use of a model in anharmonic lattice dynamics, Philos. Mag. **3**, 49 (1958).

[19] T. Tadano and S. Tsuneyuki, Self-consistent phonon calculations of lattice dynamical properties in cubic SrTiO_3 with first-principles anharmonic force constants, Phys. Rev. B **92**, 054301 (2015).

[20] G. H. O. Daalderop, P. J. Kelly, and M. F. H. Schuurmans, First-principles calculation of the magnetocrystalline anisotropy energy of iron, cobalt, and nickel, Phys. Rev. B **41**, 11919 (1990).

[21] P. Bruno, Tight-binding approach to the orbital magnetic moment and magnetocrystalline anisotropy of transition-metal monolayers, Phys. Rev. B **39**, 865 (1989).

[22] G. Kresse and D. Joubert, From ultrasoft pseudopotentials to the projector augmented-wave method, Phys. Rev. B **59**, 1758 (1999).

[23] G. Kresse and J. Furthmüller, Efficient iterative schemes for *ab initio* total-energy calculations using a plane-wave basis set, Phys. Rev. B **54**, 11169 (1996).

[24] M. Methfessel and A. T. Paxton, High-precision sampling for Brillouin-zone integration in metals, Phys. Rev. B **40**, 3616 (1989).

[25] P. E. Blöchl, O. Jepsen, and O. K. Andersen, Improved tetrahedron method for Brillouin-zone integrations, Phys. Rev. B **49**, 16223 (1994).

[26] J. P. Perdew, K. Burke, and M. Ernzerhof, Generalized Gradient Approximation Made Simple, Phys. Rev. Lett. **77**, 3865 (1996).

[27] A. Andreev, *Thermal expansion anomalies and spontaneous magnetostriction in rare-earth intermetallics with cobalt and iron*, Handbook of Magnetic Materials Vol. 8 (Elsevier, New York, 1995), Chap. 2, pp. 59–187.

[28] S. L. Dudarev, G. A. Botton, S. Y. Savrasov, C. J. Humphreys, and A. P. Sutton, Electron-energy-loss spectra and the structural stability of nickel oxide: An LSDA+U study, Phys. Rev. B **57**, 1505 (1998).

[29] D. J. Singh and L. Nordstrom, *Planewaves, Pseudopotentials, and the LAPW Method*, 2nd ed. (Springer, Berlin, 2006).

[30] K. Schwarz, P. Blaha, and G. K. Madsen, Electronic structure calculations of solids using the WIEN2k package for material sciences, Comput. Phys. Commun. **147**, 71 (2002).

[31] F. Zhou, W. Nielson, Y. Xia, and V. Ozoliņš, Lattice Anharmonicity and Thermal Conductivity from Compressive Sensing of First-Principles Calculations, Phys. Rev. Lett. **113**, 185501 (2014).

[32] T. Tadano, Y. Gohda, and S. Tsuneyuki, Anharmonic force constants extracted from first-principles molecular dynamics: applications to heat transfer simulations, J. Phys.: Condens. Matter **26**, 225402 (2014).

[33] W. Kohn and L. J. Sham, Self-consistent equations including exchange and correlation effects, Phys. Rev. **140**, A1133 (1965).

[34] J. P. Perdew, A. Ruzsinszky, G. I. Csonka, O. A. Vydrov, G. E. Scuseria, L. A. Constantin, X. Zhou, and K. Burke, Restoring

the Density-Gradient Expansion for Exchange in Solids and Surfaces, Phys. Rev. Lett. **100**, 136406 (2008).

[35] J. Sun, A. Ruzsinszky, and J. P. Perdew, Strongly Constrained and Appropriately Normed Semilocal Density Functional, Phys. Rev. Lett. **115**, 036402 (2015).

[36] A. V. Krukau, O. A. Vydrov, A. F. Izmaylov, and G. E. Scuseria, Influence of the exchange screening parameter on the performance of screened hybrid functionals, J. Chem. Phys. **125**, 224106 (2006).

[37] See Supplemental Material at http://link.aps.org/supplemental/10.1103/PhysRevB.108.014304 for details of the SCP vibrational free energy, the density of states at the Co_{2c} site computed with various exchange-correlation (XC) functionals, the smearing width dependency of the harmonic frequency and the transition temperature, the influence of using different GGA+U schemes on magnetic properties, the Co site dependence of the orbital moment and its anisotropy under the GGA+U scheme, and lattice information obtained with different XC functionals for hexagonal and orthorhombic YCo_5, which includes Refs. [57,58].

[38] G. Xing, T. Ishikawa, Y. Miura, T. Miyake, and T. Tadano, Lattice dynamics effects on finite-temperature stability of $\mathrm{R}_{1-x}\mathrm{Fe}_x$ (R = Y, Ce, Nd, Sm, and Dy) alloys from first principles, J. Alloys Compd. **874**, 159754 (2021).

[39] A. Togo and I. Tanaka, First principles phonon calculations in materials science, Scr. Mater. **108**, 1 (2015).

[40] T. Tadano and S. Tsuneyuki, First-principles lattice dynamics method for strongly anharmonic crystals, J. Phys. Soc. Jpn. **87**, 041015 (2018).

[41] T. Tadano and S. Tsuneyuki, Quartic Anharmonicity of Rattlers and Its Effect on Lattice Thermal Conductivity of Clathrates from First Principles, Phys. Rev. Lett. **120**, 105901 (2018).

[42] Y. Oba, T. Tadano, R. Akashi, and S. Tsuneyuki, First-principles study of phonon anharmonicity and negative thermal expansion in ScF_3, Phys. Rev. Mater. **3**, 033601 (2019).

[43] T. Tadano and S. Tsuneyuki, *Ab initio* prediction of structural phase-transition temperature of SrTiO_3 from finite-temperature phonon calculation, J. Ceram. Soc. Jpn. **127**, 404 (2019).

[44] R. Dronskowski and P. E. Blöchl, Crystal orbital Hamilton populations (COHP): Energy-resolved visualization of chemical bonding in solids based on density-functional calculations, J. Phys. Chem. **97**, 8617 (1993).

[45] R. Bianco, I. Errea, L. Paulatto, M. Calandra, and F. Mauri, Second-order structural phase transitions, free energy curvature, and temperature-dependent anharmonic phonons in the self-consistent harmonic approximation: Theory and stochastic implementation, Phys. Rev. B **96**, 014111 (2017).

[46] T. Tadano and W. A. Saidi, First-Principles Phonon Quasiparticle Theory Applied to a Strongly Anharmonic Halide Perovskite, Phys. Rev. Lett. **129**, 185901 (2022).

[47] H. Rosner, D. Koudela, U. Schwarz, A. Handstein, M. Hanfland, I. Opahle, K. Koepernik, M. Kuz'min, K.-H. Müller, J. Mydosh, and M. Richter, Magneto-elastic lattice collapse in YCo_5, Nat. Phys. **2**, 469 (2006).

[48] D. Koudela, U. Schwarz, H. Rosner, U. Burkhardt, A. Handstein, M. Hanfland, M. D. Kuz'min, I. Opahle, K. Koepernik, K.-H. Müller, and M. Richter, Magnetic and elastic properties of YCo_5 and LaCo_5 under pressure, Phys. Rev. B **77**, 024411 (2008).

[49] F. Zhou and V. Ozoliņš, Obtaining correct orbital ground states in f-electron systems using a nonspherical self-interaction-corrected LDA + U method, Phys. Rev. B **80**, 125127 (2009).

[50] M. Richter, Band structure theory of magnetism in 3d-4f compounds, J. Phys. D: Appl. Phys. **31**, 1017 (1998).

[51] F. Donati, Q. Dubout, G. Autès, F. Patthey, F. Calleja, P. Gambardella, O. V. Yazyev, and H. Brune, Magnetic Moment and Anisotropy of Individual Co Atoms on Graphene, Phys. Rev. Lett. **111**, 236801 (2013).

[52] J.-C. Tung, H.-R. Fuh, and G.-Y. Guo, Anomalous and spin Hall effects in hcp cobalt from GGA+U calculations, Phys. Rev. B **86**, 024435 (2012).

[53] A. I. Liechtenstein, V. I. Anisimov, and J. Zaanen, Density-functional theory and strong interactions: Orbital ordering in Mott-Hubbard insulators, Phys. Rev. B **52**, R5467 (1995).

[54] M. T. Czyżyk and G. A. Sawatzky, Local-density functional and on-site correlations: The electronic structure of $\mathrm{La}_2\mathrm{CuO}_4$ and LaCuO_3, Phys. Rev. B **49**, 14211 (1994).

[55] E. R. Ylvisaker, W. E. Pickett, and K. Koepernik, Anisotropy and magnetism in the LSDA + U method, Phys. Rev. B **79**, 035103 (2009).

[56] K. Momma and F. Izumi, *VESTA 3* for three-dimensional visualization of crystal, volumetric and morphology data, J. Appl. Crystallogr. **44**, 1272 (2011).

[57] J. Schweizer and F. Tasset, Polarised neutron study of the RCo_5 intermetallic compounds. I. The cobalt magnetisation in YCo_5, J. Phys. F: Met. Phys. **10**, 2799 (1980).

[58] A. Heidemann, D. Richter, and K. H. J. Buschow, Investigation of the hyperfine fields in the compounds LaCo_{13}, LaCo_5, YCo_5 and ThCo_5 by means of inelastic neutron scattering, Z. Phys. B: Condens. Matter **22**, 367 (1975).